FOI-R–0182–SE
October 2001
ISSN 1650-1942

Scientific report

Markus Högberg, Mattias Chevalier, Martin Berggren & Dan S. Henningson

Optimal control in wall bounded flows

Division of Aeronautics, FFA
SE-172 90 STOCKHOLM

FOI – Swedish Defence Research Agency
Division of Aeronautics, FFA
SE-172 90 STOCKHOLM

FOI-R–0182–SE
October 2001
ISSN 1650-1942

Scientific report

Markus Högberg, Mattias Chevalier, Martin Berggren & Dan S. Henningson

Optimal control in wall bounded flows

Division of Aeronautics, FFA
SE-172 90 STOCKHOLM

Abstract

Optimal control of transition in channel flow and boundary layer flow is attempted. First the optimization problem is stated and the corresponding adjoint equations used to compute the gradient of the objective function are derived for both the channel flow and boundary layer flow problems. Implementation and numerical issues are discussed. The governing equations are the incompressible Navier–Stokes equations with appropriate boundary conditions for the two cases. The boundary condition on the wall normal velocity at the walls of the channel, or at the single wall in the boundary layer case, is used as control and is determined in the iterative optimization procedure. The objective function used for the optimization problem contains the perturbation energy and a regularization term containing the control. The optimization problem is formulated using the primitive variables — velocity and pressure — and is then rewritten in a formulation containing only the wall normal velocity and the wall normal vorticity. An existing solver for the incompressible Navier–Stokes equations using this formulation can then also be used to solve the associated adjoint problem. The implementation is straightforward using this formulation and the efficiency of the original solver is maintained. To test the performance of the solver of the optimization problem, it is applied on different stages of the oblique transition scenario in the channel flow case. In a parallel Falkner–Skan–Cooke flow successful control of an inviscid instability is reported, and in the spatial Blasius flow the energy growth of a Tollmien–Schlichting wave is efficiently inhibited.

1 Introduction

In the last decade, one topic in fluid mechanics that has been subject to an increasing interest is *flow control*. The explosive development in computer technology has made it possible to approach these problems from a numerical point of view, and also to manufacture small devices to be used for measurements and actuation in experiments. The numerical approach to flow control can for example be used to design the shape of a wing to minimize drag or to solve some other optimization problem. Mathematical aspects of the flow control problem is the topic of the books edited by Gunzburger (1995) [8] and Sritharan (1998) [22]. Computational approaches to flow control are reviewed in the paper by Hinze & Kunisch (2000) [9]. Optimal control of channel flow using direct numerical simulations was previously considered using by Bewley, Moin & Temam (2001) [2] and using large eddy simulations by Collis *et al.* (2000) [5]. In addition to channel flow, Joslin *et al.* (1997) [14] also considered the boundary layer case with a two dimensional flow in direct numerical simulations.

In this work we consider the problem of control of transition from laminar to turbulent flow in a channel and a boundary layer. In many applications there is a large potential benefit from the ability to prevent transition whereas in other applications the turbulent state is the desired one. Our objective is to delay or prevent transition at low Reynolds numbers, particularly focusing on the bypass transition (Morkovin (1969) [18]), that is, transition scenarios not emanating from exponential growth of disturbances in the linearized equations. These effects are particularly important for flows involving strong shear. We refer to the recent book by Schmid & Henningson (2001) [21] for a comprehensive treatment on the subject.

2 Optimization problem formulations

The formulation of an optimal control problem is based on three important decisions. The choice of governing equations, determining what means of actuation to use, and what properties of the flow to control. For a particular flow geometry and with given fluid properties, these choices have to be made with care.

In this work the governing equations are the incompressible Navier–Stokes equations. In a recent study, successful application of feedback controllers computed from the linearized Navier–Stokes equations was performed by Högberg & Bewley (2001) [11] in temporal channel flow. Changes in the mean flow is not easily taken into account using this formulation. Thus, a proper treatment of problems where this is important, such as a flow with local separation, requires the use of the full Navier–Stokes equations.

Since no particular quantity is known that establishes where we are on the path to transition the choice of objective function is difficult. The mean skin friction drag could be used as an indicator, since it has a jump at transition, and can be used to define a transition point, as for example in Reddy *et al.* (1998) [20]. On the other hand, Bewley, Moin & Temam (2001) [2] showed that the mean drag was not a good choice for the objective function when the purpose was to relaminarize turbulence in a channel flow, and concluded that the turbulent kinetic energy was a more appropriate choice. Since we are interested in control of transition rather than turbulence, the energy of the deviation from the mean flow appears to be an appropriate quantity to minimize. An increased physical understanding of the transition process and the crucial mechanisms of turbulence could provide a guide to the best choice of objective function as pointed out by Kim & Lim (2000) [15].

It is important to choose the properties of the control in such a way that it is able to do its task in an efficient way. For our study, we have chosen to use blowing and suction at the wall during a specified period in time. The state of the flow is observed during another, possibly overlapping, period in time. When a spatially rather than a temporally evolving flow is considered, it is physically meaningful to specify also the spatial extent of the control and observation regions. The control is restricted to have zero mass flux, in order to limit the ability to affect the mean flow and focus the control effort on the perturbations.

The gradient of the objective function may be expressed in terms of the solution of an *adjoint equation*. Here, we discretize the expressions for the adjoint equations and the gradient that have been derived on the “continuous” level. An alternative is to discretize the Navier–Stokes equations and the objective function and *derive* the adjoint equations and the gradient expression on the discrete level. The latter approach leads to more accurate gradient directions, but it seems difficult to apply for the present discretizations. Issues related to the errors introduced by the approximative (continuous) formulation are discussed in e.g. Glowinski & He (1998) [6] and Gunzburger (1998) [7]. The use of the continuous formulation is motivated by the findings in Högberg & Berggren (2000) [10] where one conclusion was that it is sufficient to use the approximative (continuous) formulation in order to control strong instabilities. It was noted that in such cases most of the reduction of the objective function is achieved in the first few iterations, and additional iterations only result in a fine tuning of the control. The drawback is that it will require more iterations to reach the true optimal solution, if it is even possible, than with the discrete formulation.

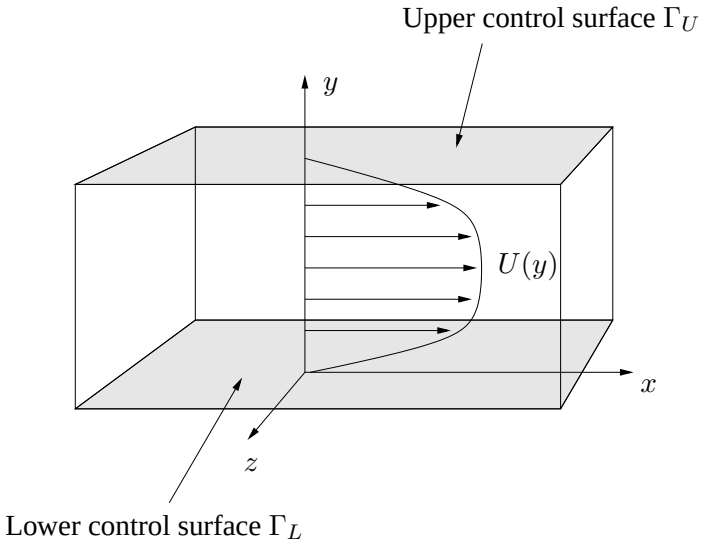

Figure 1. Geometry of flow domain Ω for channel flow simulations.

2.1 Governing equations

In this section we consider the channel flow problem and the details of the method used to solve the optimization problem. The boundary layer problem is basically an extension of the channel flow case. The differences are outlined in section 2.3, and a full description is provided in appendix A.

Our computational domain depicted in figure 1 is

$$\Omega = (-x_L/2, x_L/2) \times (-1, 1) \times (-z_L/2, z_L/2),$$

in x, y, z, and we define

$$\Gamma_L = \bar{\Omega}(y = -1), \quad \Gamma_U = \bar{\Omega}(y = 1) \quad \text{and} \quad Q = \Omega \times (0, T).$$

The non-dimensional, incompressible Navier–Stokes equations with a Reynolds number, Re, based on the centerline velocity and half the channel height are

$$\begin{cases} \dfrac{\partial u}{\partial t} + (u \cdot \nabla)u - \dfrac{1}{Re}\Delta u + \nabla\pi = -\nabla P & \text{in } Q, \\ \nabla \cdot u = 0 & \text{in } Q, \\ u|_{t=0} = u_0, \end{cases} \tag{1}$$

where $u = (u_1, v, w)$ is the velocity vector, π is the pressure and ∇P represents the pressure gradient driving the flow and can either be constant or used to ensure constant mass flux. Periodic boundary conditions in x and z, and control through blowing and suction together with a no-slip condition for the directions parallel to the wall gives the complete set of boundary conditions,

$$\begin{aligned} u|_{x=-x_L/2} &= u|_{x=x_L/2}, \\ u|_{z=-z_L/2} &= u|_{z=z_L/2}, \\ e_i \cdot u|_{y=-1} &= \begin{cases} \varphi_L^T \psi_L = \sum_{m=1}^{M_L} \varphi_{L,m}(t)\, \psi_{L,m}(x,z) & \text{in } (T_1^c, T_2^c) \quad \text{for } i = 2, \\ 0 & \text{otherwise,} \end{cases} \\ e_i \cdot u|_{y=1} &= \begin{cases} \varphi_U^T \psi_U = \sum_{m=1}^{M_U} \varphi_{U,m}(t)\, \psi_{U,m}(x,z) & \text{in } (T_1^c, T_2^c) \quad \text{for } i = 2, \\ 0 & \text{otherwise,} \end{cases} \end{aligned} \tag{2}$$

where e_i are unit basis vectors in the coordinate directions, and ψ are basis functions for the control designed to have zero net mass flux. We can now introduce the control variable φ defined as:

$$\varphi = (\varphi_L, \varphi_U)^T, \begin{cases} \varphi_L = (\varphi_{L,1}, \dots, \varphi_{L,M_L})^T, \\ \varphi_U = (\varphi_{U,1}, \dots, \varphi_{U,M_U})^T. \end{cases}$$

To completely specify the optimal control problem we also need an objective function. If we choose to minimize the energy of the deviation from a target velocity distribution, the objective function is:

$$J(\varphi) = \frac{\varepsilon}{2} \int_{T_1^c}^{T_2^c} \int_{\Gamma} |v|^2 \, \mathrm{d}\Gamma \, \mathrm{d}t + \frac{1}{2} \int_{T_1^o}^{T_2^o} \int_{\Omega} |u - u_T|^2 \, \mathrm{d}Q, \tag{3}$$

where (T_1^c, T_2^c) is the control time period and (T_1^o, T_2^o) is the observation time period. The target velocity profile is denoted u_T. The optimization problem is then: find φ^* which satisfies

$$J(\varphi^*) \leq J(\varphi) \quad \forall \; v(\varphi)|_\Gamma \in \mathcal{U}_{\text{ad}}$$

where $\mathcal{U}_{ad}$ has been used to denote the set of *admissible controls* which is a subset of $L^2((T_1^c, T_2^c); \mathbb{R}^{M_L+M_U})$.

2.2 Derivation of objective function gradient.

The gradient of the objective function ∇J is defined by

$$\begin{aligned} \delta J(\varphi) &= \lim_{s \to 0} \frac{J(\varphi + s\,\delta\varphi) - J(\varphi)}{s} = \langle \nabla J, \delta\varphi \rangle \\ &= \left\langle \frac{\partial J}{\partial \varphi_L}, \delta\varphi_L \right\rangle + \left\langle \frac{\partial J}{\partial \varphi_U}, \delta\varphi_U \right\rangle, \end{aligned} \tag{4}$$

where $\delta\varphi$ is a first variation of the control. The functional δJ is the first variation of J with respect to $\delta\varphi$. To find an expression for ∇J we start by differentiating the objective function (3) to get,

$$\delta J(\varphi) = \varepsilon \int_{T_1^c}^{T_2^c} \int_{\Gamma} \delta v \, v \, \mathrm{d}\Gamma \, \mathrm{d}t + \int_{T_1^o}^{T_2^o} \int_{\Omega} \delta u \cdot (u - u_T) \, \mathrm{d}Q, \tag{5}$$

where $\delta v = e_2 \cdot \delta u$ and δu is the first variation of u with respect to $\delta\varphi$. To find an expression for the relation between δu and $\delta\varphi$ we differentiate state equation (1),

$$\begin{cases} \dfrac{\partial \delta u}{\partial t} + (\delta u \cdot \nabla) u + (u \cdot \nabla) \delta u - \dfrac{1}{Re} \Delta \delta u + \nabla \delta\pi = 0 & \text{in } Q, \\ \nabla \cdot \delta u = 0 & \text{in } Q, \\ \delta u|_{t=0} = 0, \end{cases} \tag{6}$$

and boundary conditions (2),

$$\begin{aligned}
\delta u|_{x=-x_L/2} &= \delta u|_{x=x_L/2}, \\
\delta u|_{z=-z_L/2} &= \delta u|_{z=z_L/2}, \\
e_i \cdot \delta u|_{y=-1} &= \begin{cases} \delta\varphi_L^T \psi_L = \sum_{m=1}^{M_L} \delta\varphi_{L,m}(t)\psi_{L,m}(x,z) & \text{in } (T_1^c, T_2^c) \quad \text{for } i=2, \\ 0 & \text{otherwise,} \end{cases} \\
e_i \cdot \delta u|_{y=1} &= \begin{cases} \delta\varphi_U^T \psi_U = \sum_{m=1}^{M_U} \delta\varphi_{U,m}(t)\psi_{U,m}(x,z) & \text{in } (T_1^c, T_2^c) \quad \text{for } i=2, \\ 0 & \text{otherwise.} \end{cases}
\end{aligned} \tag{7}$$

Now we introduce a vector function $p = p(x, y, z, t)$ such that $e_i \cdot p = p_i$ and require p to satisfy the boundary conditions:

$$\begin{aligned}
p|_{x=-x_L/2} &= p|_{x=x_L/2}, \\
p|_{z=-z_L/2} &= p|_{z=z_L/2}, \\
p|_{y=-1} &= p|_{y=1} = 0.
\end{aligned} \tag{8}$$

Appropriate boundary conditions will emerge from the derivation but in order to simplify the presentation they are introduced already at this point. Taking the dot product between p and equation (6) and integrating over Q yields

$$\int_Q p \cdot \Big(\underbrace{\frac{\partial \delta u}{\partial t}}_{1} + \underbrace{(\delta u \cdot \nabla) u}_{2} + \underbrace{(u \cdot \nabla)\delta u}_{3} - \underbrace{\frac{1}{Re}\Delta \delta u}_{4} + \underbrace{\nabla \delta\pi}_{5} \Big) \, \mathrm{d}Q = 0. \tag{9}$$

Then, step by step, we apply integration by parts to move derivatives from δu to p. We start with the first term in the integral (9), containing the time derivative:

$$\begin{aligned}
\int_Q p \cdot \frac{\partial \delta u}{\partial t} \, \mathrm{d}Q &= \int_\Omega \left(p(T) \cdot \delta u(T) - p(0) \cdot \delta u(0) \right) \mathrm{d}\Omega - \int_Q \delta u \cdot \frac{\partial p}{\partial t} \, \mathrm{d}Q \\
&= \int_\Omega p(T) \cdot \delta u(T) \, \mathrm{d}\Omega - \int_Q \delta u \cdot \frac{\partial p}{\partial t} \, \mathrm{d}Q,
\end{aligned} \tag{10}$$

where we have used that $\delta u(t=0)=0$. Then consider the fourth and fifth terms in integral (9), involving $\Delta\delta u$ and $\delta\pi$:

$$
\begin{aligned}
&-\frac{1}{Re}\int_Q p\cdot\Delta\delta u\,\mathrm{d}Q+\int_Q (p\cdot\nabla)\delta\pi\,\mathrm{d}Q\\
&\quad=-\frac{1}{Re}\int_0^T\Big[\int_\Gamma \frac{\partial\delta u}{\partial n}\cdot p\,\mathrm{d}\Gamma-\int_\Omega \nabla p:\nabla\delta u\,\mathrm{d}\Omega\Big]\mathrm{d}t\\
&\qquad+\int_0^T\Big[\int_\Gamma n\cdot p\,\delta\pi\,\mathrm{d}\Gamma-\int_\Omega \delta\pi(\nabla\cdot p)\,\mathrm{d}\Omega\Big]\mathrm{d}t\\
&\quad=\int_0^T\!\!\int_\Gamma p\cdot\left(n\,\delta\pi-\frac{1}{Re}\frac{\partial\delta u}{\partial n}\right)\mathrm{d}\Gamma\mathrm{d}t\\
&\qquad+\frac{1}{Re}\int_0^T\Big[\int_\Gamma \delta u\cdot\frac{\partial p}{\partial n}\mathrm{d}\Gamma-\int_\Omega \delta u\cdot\Delta p\,\mathrm{d}\Omega\Big]\mathrm{d}t-\int_Q\delta\pi(\nabla\cdot p)\,\mathrm{d}Q\\
&\quad=\frac{1}{Re}\int_{T_1^c}^{T_2^c}\Big[\delta\varphi_L^T\int_{\Gamma_L}\psi_L\frac{\partial p_2}{\partial n}\,\mathrm{d}\Gamma+\delta\varphi_U^T\int_{\Gamma_U}\psi_U\frac{\partial p_2}{\partial n}\,\mathrm{d}\Gamma\Big]\mathrm{d}t\\
&\qquad-\frac{1}{Re}\int_Q\delta u\cdot\Delta p\,\mathrm{d}Q-\int_Q\delta\pi(\nabla\cdot p)\,\mathrm{d}Q.
\end{aligned}
\tag{11}
$$

where : denotes a complete contraction; that is,

$$
\nabla p:\nabla\delta u=\sum_{i,j=1}^{3}\frac{\partial(e_i\cdot p)}{\partial x_j}\frac{\partial(e_i\cdot\,\delta u)}{\partial x_j}.
\tag{12}
$$

In the third equality of (11), we use the boundary condition on δu from (7) and on p from (8).

We can simply rewrite the second term in (9):

$$
\int_Q p\cdot(\delta u\cdot\nabla)u\,\mathrm{d}Q=\int_Q\delta u\cdot(\nabla u)^T p\,\mathrm{d}Q.
\tag{13}
$$

For the third term in (9), we use Gauss theorem, the boundary condition on p in

(8) and the incompressibility condition,

$$\begin{aligned}
&\int_Q p \cdot (u \cdot \nabla)\delta u \,\mathrm{d}Q \\
&\quad = \int_0^T\!\!\int_\Gamma (p \cdot \delta u)(n \cdot u) \,\mathrm{d}\Gamma \,\mathrm{d}t \\
&\qquad - \int_Q (p \cdot \delta u)(\nabla \cdot u) \,\mathrm{d}Q - \int_Q \delta u \cdot (u \cdot \nabla)p \,\mathrm{d}Q \\
&\quad = -\int_Q \delta u \cdot (u \cdot \nabla)p \,\mathrm{d}Q,
\end{aligned} \tag{14}$$

Then by inserting (10), (11), (13) and (14) into (9) we get:

$$\begin{aligned}
&\int_\Omega p(T)\,\delta u(T) \,\mathrm{d}\Omega \\
&+ \frac{1}{Re}\int_{T_1^c}^{T_2^c}\left[\delta\varphi_L^T \int_{\Gamma_L} \psi_L \frac{\partial p_2}{\partial n} \,\mathrm{d}\Gamma + \delta\varphi_U^T \int_{\Gamma_U} \psi_U \frac{\partial p_2}{\partial n} \,\mathrm{d}\Gamma\right]\mathrm{d}t \\
&+ \int_Q \delta u \cdot \left(-\frac{\partial p}{\partial t} - \frac{1}{Re}\Delta p + (\nabla u)^T p - (u \cdot \nabla)p\right)\mathrm{d}Q \\
&- \int_Q \delta\pi\,(\nabla \cdot p)\,\mathrm{d}Q = 0.
\end{aligned} \tag{15}$$

If we then require p to satisfy the adjoint equations:

$$\begin{cases}
-\dfrac{\partial p}{\partial t} - \dfrac{1}{Re}\Delta p + (\nabla u)^T p \\
\qquad -(u \cdot \nabla)p + \nabla\sigma = \begin{cases} u - u_T & \text{in } (T_1^o, T_2^o) \\ 0 & \text{otherwise} \end{cases} \text{in } Q, \\
\qquad\qquad \nabla \cdot p = 0 \qquad\qquad \text{in } Q, \\
\qquad\qquad p|_{t=T} = 0,
\end{cases} \tag{16}$$

with the boundary conditions from (8) and where σ is a scalar field (the "adjoint pressure"). Then (15) becomes

$$\int_{T_1^o}^{T_2^o}\!\!\int_\Omega \delta u \cdot (u - u_T) \,\mathrm{d}Q - \int_Q \delta u \cdot \nabla\sigma \,\mathrm{d}Q = 0, \tag{17}$$

since $\partial p_2/\partial n$ is zero at the boundaries $y = \pm 1$. This follows from the fact that the no-slip condition implies

$$\frac{\partial p_1}{\partial x} = \frac{\partial p_3}{\partial z} = 0$$

on the walls and from the condition requiring p to be divergence-free. Also, note that the initial condition for the adjoint equations (16) is set at $t = T$ and that the equations are integrated backwards in time.

Integrating the second term in the integral (17) by parts yields

$$\begin{aligned} -\int_Q \delta u \cdot \nabla \sigma \, \mathrm{d}Q &= -\int_0^T\!\!\int_\Gamma n \cdot \delta u \, \sigma \, \mathrm{d}\Gamma \, \mathrm{d}t + \int_Q \sigma \, \nabla \cdot \delta u \, \mathrm{d}Q \\ &= -\int_0^T\!\!\int_\Gamma n \cdot \delta u \, \sigma \, \mathrm{d}\Gamma \, \mathrm{d}t, \end{aligned} \tag{18}$$

since $\nabla \cdot \delta u = 0$. Inserting the boundary condition on δu from (7) into (18) we get,

$$\begin{aligned} &-\int_0^T\!\!\int_\Gamma n \cdot \delta u \, \sigma \, \mathrm{d}\Gamma \, \mathrm{d}t \\ &\quad = \int_{T_1^c}^{T_2^c}\!\!\int_{\Gamma_L} \delta\varphi_L^T \psi_L \sigma \, \mathrm{d}\Gamma \, \mathrm{d}t - \int_{T_1^c}^{T_2^c}\!\!\int_{\Gamma_U} \delta\varphi_U^T \psi_U \sigma \, \mathrm{d}\Gamma \, \mathrm{d}t. \end{aligned} \tag{19}$$

If we now insert (18) and (19) into (17) we get,

$$\begin{aligned} &\int_{T_1^c}^{T_2^c} \left[\delta\varphi_L^T \int_{\Gamma_L} \psi_L \sigma \, \mathrm{d}\Gamma - \delta\varphi_U^T \int_{\Gamma_U} \psi_U \sigma \, \mathrm{d}\Gamma \right] \mathrm{d}t \\ &\quad + \int_{T_1^o}^{T_2^o}\!\!\int_\Omega \delta u \cdot (u - u_T) \, \mathrm{d}Q = 0. \end{aligned} \tag{20}$$

Finally we can now insert (20) into (5) using (2) to eliminate δu

$$\begin{aligned} \delta J(\varphi) &= \left\langle \frac{\partial J}{\partial \varphi_L}, \delta\varphi_L \right\rangle + \left\langle \frac{\partial J}{\partial \varphi_U}, \delta\varphi_U \right\rangle \\ &= \int_{T_1^c}^{T_2^c} \Big\{ \delta\varphi_L^T \Big[\int_{\Gamma_L} \psi_L \left(\varepsilon \varphi_L^T \psi_L - \sigma \right) \mathrm{d}\Gamma \Big] \\ &\qquad + \delta\varphi_U^T \Big[\int_{\Gamma_U} \psi_U \left(\varepsilon \varphi_U^T \psi_U + \sigma \right) \mathrm{d}\Gamma \Big] \Big\} \mathrm{d}t. \end{aligned} \tag{21}$$

From expression (21) we can identify the gradient of the objective function (3),

$$\frac{\partial J}{\partial \varphi_L} = \int_{\Gamma_L} \psi_L \left(\varepsilon \varphi_L^T \psi_L - \sigma \right) \mathrm{d}\Gamma, \tag{22}$$

and

$$\frac{\partial J}{\partial \varphi_U} = \int_{\Gamma_U} \psi_U \left(\varepsilon \varphi_U^T \psi_U + \sigma \right) \mathrm{d}\Gamma. \tag{23}$$

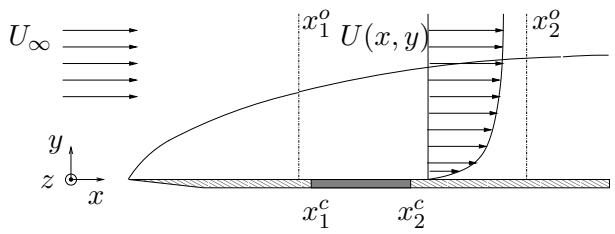

Figure 2. Geometry for boundary layer flow simulations.

Note that these gradients are vector-valued (dimensions M_L and M_U) functions of time.

2.3 Extension to boundary layer

Only minor changes are needed to rephrase the channel flow problem to the boundary layer flow depicted in figure 2. A complete derivation of the boundary layer counterpart of the channel flow optimization problem can be found in appendix A. In this section only the key differences will be pointed out and commented.

The growing boundary layer is modeled by

$$\begin{cases} \dfrac{\partial u}{\partial t} + (u \cdot \nabla)u - \dfrac{1}{Re}\Delta u + \nabla \pi = \lambda(x)(U-u) & \text{in } Q, \\ \nabla \cdot u = 0 & \text{in } Q, \\ u|_{t=0} = u_0, \end{cases} \tag{24}$$

with periodic boundary conditions in the horizontal directions, that is, the x- and z-directions,

$$\begin{aligned} u|_{x=-x_l/2} &= u|_{x=x_l/2}, \\ u|_{z=-z_l/2} &= u|_{z=z_l/2}. \end{aligned} \tag{25}$$

The term $\lambda(x)(U-u)$ is a forcing term used to make the flow situation sketched in figure 2 periodic, enabling the use of Fourier discretization in simulations of the physical flow. This is known as the fringe region technique and is described further in Lundbladh *et al.* (1999) [17] and analyzed by Nordström, Nordin & Henningson (1999) [19]. Left to be specified are the conditions on the wall and in the free-stream. On the wall, the boundary condition for the horizontal velocities is a non-slip condition, whereas the wall normal velocity v_c is given by the control. The free-stream condition is that $u \to (U_\infty, 0, W_\infty)$ as $y \to \infty$. We may thus specify

$$\begin{aligned} u|_{\Gamma_u} &= (U_\infty, 0, W_\infty), \\ u|_{\Gamma_c} &= n v_c, \\ u_{\Gamma_l \setminus \Gamma_c} &= 0, \end{aligned} \tag{26}$$

where Γ_u and Γ_l represent the upper and lower part of the boundary respectively. The part of the boundary where the control is applied is denoted Γ_c.

In the code there are numerous, alternative, less intrusive choices for the free-stream condition than the Dirichlet condition above, in order to keep the height

of the box as small as possible. The one that is actually used for the numerical experiments is

$$\left.\frac{\partial u}{\partial n}\right|_{\Gamma_u} = 0. \tag{27}$$

As for the channel flow case we expand the control v_c in basis functions $\psi_{l,m}$ with zero mass flux, where $\varphi_{l,m}$ are time dependent coefficients for the basis functions,

$$v_c(x,z,t) = \begin{cases} \varphi_l^T \psi_l = \displaystyle\sum_{m=1}^{M} \varphi_{l,m}(t)\psi_{l,m}(x,z) & \text{in } (T_1^c, T_2^c), \\ 0 & \text{otherwise.} \end{cases} \tag{28}$$

Where we have introduced the control vector φ_l defined as:

$$\varphi_l = (\varphi_{l,1}, \ldots, \varphi_{l,M}).$$

Comparing with the corresponding equation for channel flow, equation (1) and the associated boundary conditions, there are two differences. The boundary condition at the upper wall is now replaced by a free-stream velocity condition. Also the aforementioned fringe forcing term which is needed only for spatial simulations is added to the right hand side. The scalar function $\lambda = \lambda(x)$ is nonzero only in the fringe region and is defined as follows:

$$\lambda(x) = \lambda_{\max}\left[S\left(\frac{x - x_{\text{start}}}{\Delta_{\text{rise}}}\right) - S\left(\frac{x - x_{\text{end}}}{\Delta_{\text{fall}}} + 1\right)\right]$$

where $\lambda_{\max}$, x_{start}, x_{end}, Δ_{rise} and Δ_{fall} are parameters used to specify the strength, extent and shape of the fringe forcing. The S-function is defined as

$$S(r) = \begin{cases} 0 & r \le 0, \\ \dfrac{1}{1 + \exp(1/(1-r) + 1/r)} & 0 < r < 1, \\ 1 & r \ge 1. \end{cases}$$

Another difference from the channel flow problem formulation appears in the second term of the objective function J, equation (3), where the observation of state can now be limited in space as well as in time which yields,

$$J(\varphi_l) = \frac{\varepsilon}{2}\int_{T_1^c}^{T_2^c}\int_{\Gamma_c} |v_c|^2 \,\mathrm{d}\Gamma\,\mathrm{d}t + \frac{1}{2}\int_{T_1^o}^{T_2^o}\int_{\Omega_o} |u - u_T|^2 \,\mathrm{d}Q, \tag{29}$$

where (T_1^c, T_2^c) is the control time period and (T_1^o, T_2^o) is the observation time period and Ω_o is the part of the spatial domain Ω where the state of the flow is observed. This is only used for spatial simulations.

As for the channel flow derivation, we get to the stage where the adjoint equations with the variables p and σ are introduced:

$$\begin{cases} -\dfrac{\partial p}{\partial t} + (\nabla u)^T p - (u \cdot \nabla) p \\ \quad -\dfrac{1}{Re}\Delta p + \lambda(x) p + \nabla \sigma = \begin{cases} u - u_T & \text{in } (T_1^o, T_2^o) \times \Omega_o \\ 0 & \text{otherwise} \end{cases} \text{in } Q, \\ \nabla \cdot p = 0 \qquad \text{in } Q, \\ p|_{t=T} = 0. \end{cases} \tag{30}$$

along with the boundary conditions:

$$\begin{aligned} p|_{x=-x_l/2} &= p|_{x=x_l/2}, \\ p|_{z=-z_l/2} &= p|_{z=z_l/2}, \\ p|_{\Gamma_l} &= 0, \\ p|_{\Gamma_u} &= 0, \end{aligned} \tag{31}$$

The solution to the adjoint equations will vanish far above plate, so the condition at Γ_u may be regarded as a zero free-stream condition for the adjoint equations. Following the same reasoning as for the free-stream condition in the Navier–Stokes equation, we actually use the Neumann condition

$$\left.\frac{\partial p}{\partial n}\right|_{\Gamma_u} = 0. \tag{32}$$

instead for the zero Dirichlet condition in the numerical experiments. It is possible instead to use the exact adjoint boundary condition associated to the Neumann condition (27). However, this would substantially complicate the implementation, since the pressure is not easily available with the current solution procedure (see section 3.1).

Due to the fringe forcing, the additional term $\lambda(x)p$ will appear in the adjoint equations. The forcing $u - u_T$ is now confined to the spatial domain Ω_o due to the variable spatial extent of the observation. These adjustments lead to following the expression for the gradient:

$$\frac{\partial J}{\partial \varphi_l} = \int_{\Gamma_c} \psi_l \left(\varepsilon \varphi_l^T \psi_l - \sigma \right) \mathrm{d}\Gamma. \tag{33}$$

3 Adapting to the simulation codes

3.1 Reformulation of the adjoint equations

To be able to use existing spectral channel flow and boundary layer flow codes by Lundbladh, Henningson & Johansson (1992) [16] and Lundbladh *et al.* (1999) [17] respectively, we need to reformulate the adjoint equations into a similar form to the one used there. The simulation code for the boundary layer problem is based on the channel flow code and the solution procedure is identical. The Navier–Stokes equations are implemented in a $v-\omega$ formulation, where linear and non-linear terms are treated separately. We can write the adjoint equations (16) or (30) as

$$\begin{cases} -\dfrac{\partial p}{\partial t} - \dfrac{1}{Re}\Delta p - H + \nabla(u\cdot p) + \nabla\sigma = 0, \\ \nabla\cdot p = 0, \\ p|_{t=T} = 0, \end{cases} \tag{34}$$

with the boundary conditions (8) or (31), and where H in the following denotes either H_{ch} or H_{bl} corresponding to the forcing terms in the channel and boundary layer cases respectively. In order to avoid derivatives of u in the adjoint equations, terms involving such derivatives are reformulated. Using the identity

$$u\times(\nabla\times p) - 2(\nabla p)^T u + \nabla(u\cdot p) = (\nabla u)^T p - (u\cdot\nabla)p$$

the forcing in the channel flow case is given by

$$H_{ch} = -u\times(\nabla\times p) + 2(\nabla p)^T u + \begin{cases} u - u_T & \text{in } (T_1^o, T_2^o), \\ 0 & \text{otherwise,} \end{cases}$$

and in the boundary layer case we use

$$H_{bl} = -u\times(\nabla\times p) + 2(\nabla p)^T u - \lambda(x)p + \begin{cases} u - u_T & \text{in } (T_1^o, T_2^o)\times\Omega_o, \\ 0 & \text{otherwise,} \end{cases}$$

but apart from this, the procedure is the same in both cases. If we take the divergence of equation (34) we get a Poisson equation for the adjoint pressure:

$$\Delta\sigma = \nabla\cdot H - \Delta(u\cdot p). \tag{35}$$

We can then apply the Laplace operator to equation (34), take the second component, and combine with (35) to get:

$$-\frac{\partial\Delta p_2}{\partial t} - \frac{1}{Re}\Delta^2 p_2 - \left(\frac{\partial^2}{\partial x^2} + \frac{\partial^2}{\partial z^2}\right)H_2 + \frac{\partial}{\partial y}\left(\frac{\partial H_1}{\partial x} + \frac{\partial H_3}{\partial z}\right) = 0. \tag{36}$$

Then we take the second component of the equation obtained by taking the curl of equation (34) and again making use of (35) to get,

$$-\frac{\partial(\nabla\times p)_2}{\partial t} - \frac{1}{Re}\Delta(\nabla\times p)_2 - \left(\frac{\partial H_1}{\partial z} - \frac{\partial H_3}{\partial x}\right) = 0. \tag{37}$$

We can write equation (36) as a system of two second order equations:

$$\begin{cases} -\dfrac{\partial \phi}{\partial t} = h_{p_2} + \dfrac{1}{Re}\Delta\phi, \\ \Delta p_2 = \phi, \\ p_2(y=\pm 1) = \dfrac{\partial p_2}{\partial y}(y=\pm 1) = 0, \end{cases} \tag{38}$$

where

$$h_{p_2} = \left(\frac{\partial^2}{\partial x^2} + \frac{\partial^2}{\partial z^2}\right) H_2 - \frac{\partial}{\partial y}\left(\frac{\partial H_1}{\partial x} + \frac{\partial H_3}{\partial z}\right). \tag{39}$$

Written on the same form equation (37) reads:

$$\begin{cases} -\dfrac{\partial (\nabla \times p)_2}{\partial t} = h_{(\nabla \times p)_2} + \dfrac{1}{Re}\Delta(\nabla \times p)_2, \\ (\nabla \times p)_2(y=\pm 1) = 0, \end{cases} \tag{40}$$

where

$$h_{(\nabla \times p)_2} = \left(\frac{\partial H_1}{\partial z} - \frac{\partial H_3}{\partial x}\right). \tag{41}$$

Equations (38), (39), (40) and (41) are identical to those solved by the spectral channel flow and boundary layer codes with slight changes to H and a negative time derivative. Since the adjoint equations are solved backwards in time, we can in practice use the same solver.

3.2 Gradient evaluation

In the gradient of the objective function we need the adjoint pressure at the wall. This is not available directly since we have eliminated the adjoint pressure term from the equations, and thus the pressure is not computed explicitly. If we evaluate equation (16) or (30) at the walls, we get

$$\begin{aligned} \sigma_x\Big|_W &= \frac{1}{Re}\frac{\partial^2 p_1}{\partial y^2}\Big|_W + v\frac{\partial p_1}{\partial y}\Big|_W, \\ \sigma_z\Big|_W &= \frac{1}{Re}\frac{\partial^2 p_3}{\partial y^2}\Big|_W + v\frac{\partial p_3}{\partial y}\Big|_W, \end{aligned} \tag{42}$$

where W denotes the value at the wall and v is the wall normal velocity at the wall, or rather the control input. Note that in the channel flow case there are two walls and in the boundary layer flow there is only one. Since the constant part of the adjoint pressure disappears in the integral over the basis functions ψ in (22) and (23) we can compute the objective function gradient by integration of these adjoint pressure gradients at the wall.

4 Implementation issues

4.1 Simulation codes

The implementation of the adjoint solver is based on existing direct numerical simulation codes for channel and boundary layer flow. These codes have been extensively used and are thoroughly verified. The channel flow code is described in Lundbladh, Henningson & Johansson (1992) [16] and the boundary layer code in Lundbladh *et al.* (1999) [17]. The time marching is performed with a Runge–Kutta method for advective terms and a Crank–Nicolson scheme for the viscous terms. A spectral method described in Canuto *et al.* (1988) [4] is used with a Fourier discretization in x and z, and a Chebyshev method in y. The discretization of, and the solution procedure for, the Navier–Stokes equations is described in Lundbladh, Henningson & Johansson (1992) [16]. The adjoint equation is solved in exactly the same way, with the formulation of the equations described in section 3.1. For the boundary layer case the code described in Lundbladh *et al.* (1999) [17] is used and since it is based on the channel flow code the implementation is similar.

The solution of the adjoint equations require knowledge about the full state in space and time from the solution of the Navier–Stokes system. This is achieved by saving a large number of velocity fields equidistant in time and interpolating linearly in time when the adjoint equations are solved. This introduces an error, but if the time step between saved field is small enough, we expect a sufficiently accurate approximation. The number of saved velocity fields can become large especially if the time domain is long. An efficient way of reducing the memory requirement is to use a check-pointing technique, see for example Berggren (1998) [1]. This decreases the memory requirement at the cost of increased computational time. For the simple test cases presented in this paper check-pointing has not been necessary, but for larger cases, especially simulations requiring high spatial resolution, it will be needed.

4.1.1 Implementation of control

The control is implemented as the Fourier coefficients of the v velocity at the wall(s). The control function is discretized in time with a fixed time step that can be used to change the time resolution of the control and there is one set of coefficients for each control time. Linear interpolation is used for the control in times between the discrete control times. The control always starts and ends with zero velocity, and has zero mass flux. The time step in the solution of both the forward and adjoint equations is adjusted to be small enough to at least resolve the control in time, even if the time step allowed for numerical stability is larger.

When simulating a spatial boundary layer the control is applied only on Γ_c which extends over the interval (x_1^c, x_2^c) in the chordwise direction. In the code a filtering is added to handle this and to enforce the zero mass flux condition on the control,

$$\int_{\Gamma_l} v_c \, \mathrm{d}\Gamma = 0. \tag{43}$$

The control is then modified to have zero velocity outside Γ_c,

$$\int_{\Gamma_l} \tilde{\varphi}_l^T \psi_l \, \mathrm{d}\Gamma = \int_{\Gamma_l} (\varphi_l^T \psi_l + c)\chi(x_1^c, x_2^c) \, \mathrm{d}\Gamma = 0 \tag{44}$$

which yields,

$$c = -\frac{\int_{\Gamma_l} \varphi_l^T \psi_l \, \chi(x_1^c, x_2^c) \, \mathrm{d}\Gamma}{\int_{\Gamma_l} \chi(x_1^c, x_2^c) \, \mathrm{d}\Gamma}, \tag{45}$$

and where $\chi(r_1, r_2) = \chi[r_1, r_2](r)$ is defined as:

$$\chi[r_1, r_2](r) = \begin{cases} 1 & \text{if } r \in (r_1, r_2), \\ 0 & \text{otherwise.} \end{cases} \tag{46}$$

The procedure for modifying the control can be summarized as follows:

$$\hat{\varphi}_l \xrightarrow{\text{inverse FFT}} \varphi_l \xrightarrow{\text{Filtering and mass flux correction}} \tilde{\varphi}_l \xrightarrow{\text{FFT}} \hat{\tilde{\varphi}}_l$$

assuming that we denote the original Fourier space control with $\hat{\varphi}_l$ and the final control in Fourier space with $\hat{\tilde{\varphi}}_l$. This final control constitutes the boundary condition in the simulation when the spatial extent of the control is limited.

4.1.2 Computing the objective function gradient

The gradient of the objective function is evaluated from the adjoint pressure on the walls as described in section 3.2. When the adjoint equations are solved, the adjoint pressure on the walls must also be computed simultaneously in the control interval. Since the p_1 and p_3 velocities are available at each time step we can compute the pressure gradients σ_x and σ_z using (42). The corresponding pressure is then computed by integrating these gradients with the constant part of the adjoint pressure set to zero, since it does not enter the gradient computation. The adjoint pressure is then projected onto the basis functions of the control using (22), (23) or (33). In the spatial boundary layer case the gradient (33) is computed in Fourier space, but we should only integrate over Γ_c. The gradient is transformed to physical space and there a step function which cuts out the region Γ_c is applied. This filtering procedure is similar to that for the control. The resulting gradient is then transformed back to Fourier space.

4.2 Optimization routine

Optimization is performed with a limited memory quasi-Newton method. The algorithm, L-BFGS-B (Byrd *et al.* (1994) [3]), is available on the Internet (the web-link is given in the reference list next to Byrd *et al.* (1994) [3]) and was downloaded and compiled without modifications. It is an algorithm well suited for large non-linear optimization problems, with or without bounds on the control variables. The BFGS method uses an approximation of the Hessian matrix of the

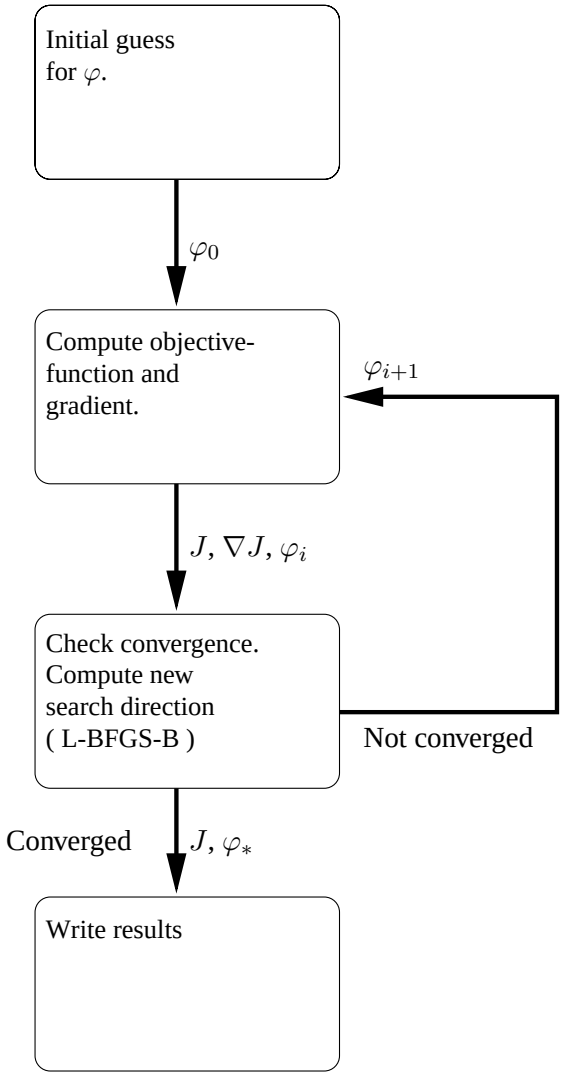

Figure 3. The flow in the optimization with L-BFGS-B.

objective function, instead of the full matrix. The algorithm has been shown to work well for many different types of optimization problems. The flow of the optimization process is described in figure 3. The limited memory BFGS algorithm differs from the standard BFGS algorithm in that Hessian approximations are build from a fixed number of gradients and control updates from earlier optimization iterations. This number is then much smaller — say 5–10 — than the order of the Hessian matrix, which may be of the order of hundred thousand for the current problem. Consult Byrd *et al.* (1994) [3] for details. The inputs to the optimization routine are the control, the gradient of the control and the value of the objective function. A new control is then obtained as output and applied in the next iteration until the convergence criterion has been met. There are a few different convergence criteria that can be used simultaneously or separately such as the norm of the gradient and the relative reduction of the objective function between iterations.

5 Results

5.1 Gradient accuracy

To verify that the implementation is correct as well as that the problem has been formulated correctly, one can check the accuracy of the gradient of the objective function. By perturbing one degree of freedom of the control and computing the resulting change in the objective function the gradient with respect to that degree of freedom can be approximated. Performing this procedure for all degrees of freedom gives the complete objective function gradient. The gradient so computed can then be used to verify that the gradient obtained from the adjoint equation approach is correct. This has been done at different stages of the optimization process for a number of different cases, varying the flow perturbation as well as the initial guess for the control. The accuracy of the gradient direction is quantified by normalizing the two gradients and computing the norm of the difference between them. This difference is less than 1% for all channel and boundary layer flow cases tested when the optimization routine is in the initial iterations. When the gradient accuracy is computed for solutions close to the optimal solution, the accuracy is degraded and the error can be as large as $10\% - 20\%$. This degraded accuracy is expected when using the current approach. In order to keep the accuracy of gradient directions also for small values of the gradient, one would need to calculate the exact gradient of the discrete objective function, and to take into account the form of the free-stream conditions that is actually used (cf. section 2.3). It is questionable, however, to what extent this is possible with the current discretization and solution method. The current approach can thus be expected to work well when there is a sufficiently high sensitivity on the objective function to changes in the control, something that is reasonable to assume for transition phenomena. However, when the sensitivity is low, the gradient will be small, and the optimization convergence may be slow.

5.2 Control of oblique transition in channel flow

As a first test case, we study the oblique transition scenario. Oblique waves are introduced in the flow, where they grow and induce streamwise vortices. The vortices then produce streamwise streaks that grow until they finally break down and transition occurs. The threshold energies for this type of bypass transition are studied in Reddy *et al.* (1998) [20]. The initial stage of this scenario is the growth of oblique waves. If the amplitude is low, this is all that happens before the flow returns to the laminar state. With a higher amplitude, the oblique waves induce enough streamwise vorticity to generate streaks. The streaks grow to a much higher amplitude than the oblique waves. If the initial disturbance is large enough, we get transition to turbulence.

Testing the optimal control on this scenario is done at three different stages and with different time resolution. First, control is applied at the very beginning where only the oblique waves are present. Second, the control is applied in the beginning of the streak growth, where both streaks and oblique waves are present. In the last case, the control is applied to the growing streaks. The results in this section were previously reported in Högberg, Henningson & Berggren (2000) [13].

Five different simulations are performed using the same initial condition. The

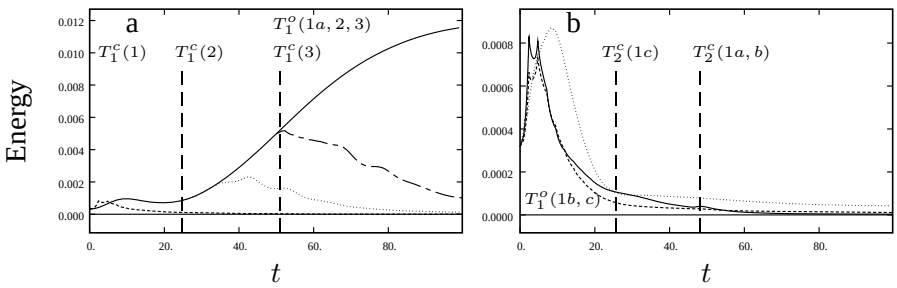

Figure 4. [a] Solid: the energy growth without control ; dashed: case 1a ; dotted : case 2 ; dash-dot: case 3. [b] solid: case 1a ; dashed: case 1b ; dotted: case 1c.

objective is to minimize the integral of the deviation from the laminar flow profile from time T_1^o to $T_2^o = 100$. The Reynolds number is 1500 and the box size is $2\pi \times 2 \times 2\pi$ in x, y, z. In case 1a,b,c the control is applied from time $T_1^c = 0$ until $T_2^c = 50$ in a,b and $T_2^c = 25$ in c. The objective function is measured from $T_1^o = 50$ in case 1a and from $T_1^o = 0$ in cases 1b and 1c. For cases 2 and 3 the control is applied from $T_1^c = 25$ and $T_1^c = 50$ respectively, and the objective function from $T_1^o = 50$. The resulting control velocity in all cases is of the order 2% of the centerline velocity. The reduction of the gradient norm is about three orders of magnitude after 10–15 optimization iterations.

The energy evolution of the controlled flows is shown in figure 4a. The growth of the oblique waves is efficiently hindered by the control formulation in 1a,b,c and the growth of streaks is eliminated also in cases 2 and 3. In case 2 the control is applied during the formation of the streaks. Initially the energy is allowed to grow but then the growth is hindered by the control and energy decays as. In case 3 the streaks have formed and are growing when control is applied.

In figure 4b the differences between the controlled flows in cases 1a,b and c are shown. In case 1a the energy is not penalized by the objective function initially as it is in 1b, and this results in lower energy after $t = 50$ than in case 1b. A higher temporal resolution of the control is applied during a shorter time in case 1c. The result is a smoother energy curve but not as low energy at a later time as in the other two cases.

5.3 Control in a parallel boundary layer flow

In order to evaluate this type of control strategy for a parallel boundary layer flow we consider an inviscid instability. Inviscid instabilities can exist only if the velocity profile has an inflection point. In a boundary layer flow with a three-dimensional velocity profile, there is always a direction in which such an inflection point exists. In this direction an unstable eigenvalue to the linearized problem was found. The corresponding eigenmode is added to an undisturbed base flow, and the sum is then used as the initial velocity field for the simulations. The base flow is chosen as a Falkner–Skan–Cooke (FSC) flow with the same parameters as are used in the investigation by Högberg & Henningson (2001) [12] where the Reynolds number is $Re_{\delta_0^*} = 337.9$. The spatial variation of the chordwise mean flow is given through,

$$U_\infty = \left(\frac{x}{x_0} + 1\right)^m,$$

where $x_0 = 354.0$. Furthermore, the cross-flow velocity was $W_\infty = 1.44232$ and $m = 0.34207$. The box dimensions for our simulations are $25.14 \times 20 \times 25.14$ measured in δ^* with a resolution of $4 \times 129 \times 4$ in $x \times y \times z$ respectively. The

resolution in the y-direction is chosen fairly large to ensure high accuracy for the y-derivatives needed in the adjoint computation.

For the temporal simulation we use the Falkner–Skan–Cooke flow at $x = 0$. The eigenvalue of the mode used in the simulation is $\omega = (-0.15246 + i0.0382)$, for the parameter choice $\alpha = 0.25$, $\beta = -0.25$. The control is applied from $T_1^c = 0$ to $T_2^c = 150$ and over the entire boundary ($\Gamma_c = \Gamma_l$). The objective function is measured from $T_1^o = 0$ to $T_2^o = 150$ and over the whole spatial domain ($\Omega_o = \Omega$).

Figure 5 shows the disturbance energy growth due to the eigenmode and also the result when the optimal control is applied. As we can see from the figure, the exponential energy growth is stopped almost immediately by the control. The first energy peak is mostly due to the energy expenditure to exert control. The maximum magnitude of the control is of the order of 0.02% of the free-stream velocity. The gradient norm is reduced about two orders of magnitude after 5–10 optimization iterations.

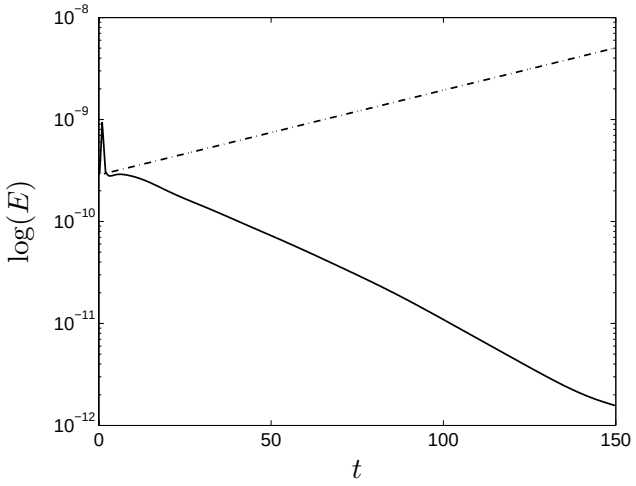

Figure 5. Solid: the disturbance energy growth with optimal control ; dash-dot: the disturbance energy growth for temporal FSC flow without control.

5.4 Control in a spatial boundary layer flow

A more general flow case to study is when we let the boundary layer grow in the chordwise direction. For this case we have chosen to study a Tollmien–Schlichting (TS) wave in a Blasius boundary layer. The dimensions of the simulation box are $200 \times 20 \times 10$ measured in δ_0^* with a resolution of $96 \times 129 \times 4$ in $x \times y \times z$ respectively. The TS wave is triggered by an oscillating volume force at $x = 10$ which is slightly upstream of branch I, located at $x \approx 40$ where it becomes unstable. The volume forcing does not introduce a pure TS eigenmode into the flow and this will result in a varying growth of the total energy of the perturbation.

The control is allowed to be active between $T_1^c = 0$ and $T_2^c = 400$ and is located on $\Gamma_c = (20, 70) \times (-5, 5)$. The control is localized in space to give us a region to observe its action downstream of the control area.

The observation time interval is also limited to give the control enough freedom to act initially since we are more interested in the final results. Thus, the objective function is measured from $T_1^o = 380$ to $T_2^o = 400$ over the domain $\Omega_o = (20, 150) \times (0, 20) \times (-5, 5)$ that includes only the physical solution meaning that the fringe region is omitted.

Without the control we can see how the disturbance energy grows in figure 6, whereas with the optimal control applied on Γ_c the energy growth is efficiently interrupted.

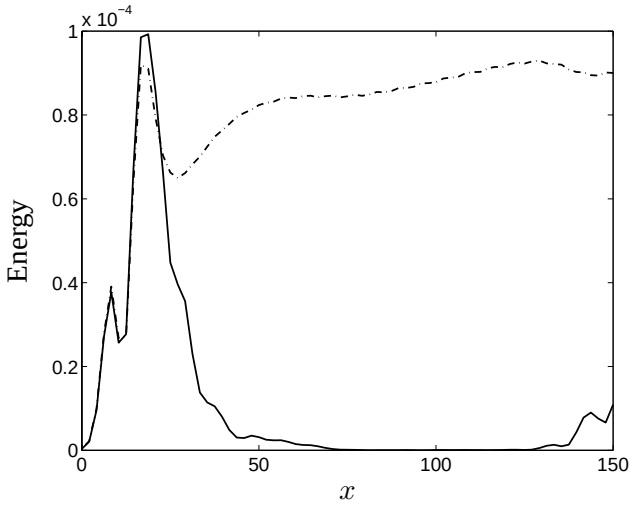

Figure 6. Solid: the disturbance energy growth with optimal control ; dash-dot: the disturbance energy growth for a spatial Blasius boundary layer flow without control.

6 Summary and conclusions

First we conclude that optimal control of transition appears to be possible to compute with the approximative discretized adjoint technique used in this work. This was also what the preliminary study by Högberg & Berggren (2000) [10] suggested. In addition, the optimization problem was derived using the primitive variables velocity and pressure but solved using a velocity–vorticity formulation. This made it easy to implement a solver for the adjoint equations using already developed codes as templates. The adjoint solver thus benefited from the efforts put into making the existing codes computationally efficient.

The optimization routine BFGS by Byrd *et al.* (1994) [3] was found to perform well for the present optimization problems. No modification of the code was necessary.

The test cases for the boundary layer code provide confirmation that this kind of optimization problem is tractable. From the simple parametric study of control of oblique waves in channel flow we can draw a few conclusions.

- The temporal extent of the control appears to be more important than the resolution.
- Allowing a higher energy initially can result in lower energy at a later time.
- It appears that there is enough control authority using blowing and suction on the wall to handle all the different stages of the oblique transition scenario.
- The choice of objective function in terms of time intervals is very important for the performance of the resulting control.

The simple flow cases studied to test the code can now be replaced with more complicated flows. In particular flows where non-linear effects are dominating are of interest, and so are flows with spatial variations in the mean flow profile.

Appendix A

Derivation of gradient for boundary layer flows

A.1 The governing equations

The domain where we solve the governing equations, given $0 < T < +\infty$, is

$$\begin{aligned} \Omega &= (-x_l/2, x_l/2) \times (0, y_l) \times (-z_l/2, z_l/2), \\ Q &= \Omega \times (0, T). \end{aligned} \tag{47}$$

The boundary of Ω is denoted Γ, and

$$\Gamma_l = \bar{\Omega}(y = 0), \quad \Gamma_u = \bar{\Omega}(y = y_l), \tag{48}$$

and $\Gamma_c \subset \Gamma_l$ represents the part of the lower boundary where control is applied. For temporal simulations Γ_c coincide with Γ_l.

The governing equations for boundary layer flow are the same as for the channel flow except for an extra term which is added to enforce periodicity of the physical flow in the streamwise direction. This is only needed for spatial simulations.

$$\begin{cases} \dfrac{\partial u}{\partial t} + (u \cdot \nabla)u - \dfrac{1}{Re}\Delta u + \nabla \pi = \lambda(x)(U - u) & \text{in } Q, \\ \nabla \cdot u = 0 & \text{in } Q, \\ u|_{t=0} = u_0, \end{cases} \tag{24}$$

with periodic boundary conditions in the horizontal directions, that is, the x- and z-directions,

$$\begin{aligned} u|_{x=-x_l/2} &= u|_{x=x_l/2}, \\ u|_{z=-z_l/2} &= u|_{z=z_l/2}. \end{aligned} \tag{25}$$

Left to be specified are the conditions in the free-stream and on the wall,

$$\begin{aligned} u|_{\Gamma_u} &= (U_\infty, 0, W_\infty), \\ u|_{\Gamma_c} &= nv_c, \\ u_{\Gamma_l \setminus \Gamma_c} &= 0. \end{aligned} \tag{26}$$

However, in the code the Neumann boundary condition

$$\left.\frac{\partial u}{\partial n}\right|_{\Gamma_u} = 0. \tag{27}$$

is used as the free-stream condition. See section 2.3 for more details regarding the free-stream boundary condition.

In equation (24), $U = U(x, y)$ is the velocity field that we force the solution towards in the fringe region. Pressure is denoted π and the Reynolds number Re is defined based on the free-stream velocity and the displacement thickness δ^*.

The scalar function $\lambda = \lambda(x)$ is nonzero only in the fringe region and is defined as follows:

$$\lambda(x) = \lambda_{\max}\left[S\left(\frac{x - x_{\text{start}}}{\Delta_{\text{rise}}}\right) - S\left(\frac{x - x_{\text{end}}}{\Delta_{\text{fall}}} + 1\right)\right],$$

where $\lambda_{\max}$, x_{start}, x_{end}, Δ_{rise} and Δ_{fall} are parameters used to specify the strength, extent and shape of the fringe forcing. The S-function is defined as,

$$S(r) = \begin{cases} 0 & r \leq 0, \\ \dfrac{1}{1 + \exp(1/(1-r) + 1/r)} & 0 < r < 1, \\ 1 & r \geq 1. \end{cases}$$

As for the channel flow case we expand the control v_c in basis functions $\psi_{l,m}$ with zero mass flux, and where $\varphi_{l,m}$ are time dependent coefficients for the basis functions,

$$v_c(x,z,t) = \begin{cases} \varphi_l^T\, \psi_l = \displaystyle\sum_{m=1}^{M} \varphi_{l,m}(t)\psi_{l,m}(x,z) & \text{in } (T_1^c, T_2^c), \\ 0 & \text{otherwise.} \end{cases} \tag{28}$$

Where we have introduced the control vector φ_l defined as:

$$\varphi_l = (\varphi_{l,1}, \ldots, \varphi_{l,M}).$$

A.2 The objective function

We minimize the deviation energy from a given target velocity distribution u_T and add a regularization term including an $\varepsilon > 0$:

$$J(\varphi_l) = \frac{\varepsilon}{2}\int_{T_1^c}^{T_2^c}\int_{\Gamma_c} |v_c|^2 \,\mathrm{d}\Gamma\,\mathrm{d}t + \frac{1}{2}\int_{T_1^o}^{T_2^o}\int_{\Omega_o} |u - u_T|^2 \,\mathrm{d}Q, \tag{29}$$

where (T_1^c, T_2^c) is the control time period and (T_1^o, T_2^o) is the observation time period and Ω_o is the part of the domain Ω where the state of the flow is observed. The control problem can now be defined as:

$$\begin{gathered} \text{Find } \varphi^* \in \mathcal{U}_{\text{ad}} \text{ such that} \\ J(\varphi^*) \leq J(\varphi_l) \quad \forall\ v_c(\varphi_l) \in \mathcal{U}_{\text{ad}}, \end{gathered} \tag{49}$$

where φ^* is the optimal control. The set of admissible controls is denoted $\mathcal{U}_{\text{ad}}$ and is a subset of $L^2((T_1^c, T_2^c); \mathbb{R}^M)$.

A.3 Derivation of the objective function gradient

We begin by differentiating the objective function (29)

$$\delta J(\varphi_l) = \varepsilon\int_{T_1^c}^{T_2^c}\int_{\Gamma_c} \delta v_c\, v_c \,\mathrm{d}\Gamma\,\mathrm{d}t + \int_{T_1^o}^{T_2^o}\int_{\Omega_o} \delta u \cdot (u - u_T) \,\mathrm{d}Q, \tag{50}$$

where the gradient of J is defined through the directional derivative of J in the $\delta\varphi_l$-direction as done in (4). The differentiated Navier–Stokes equations have the form

$$\begin{cases} \dfrac{\partial \delta u}{\partial t} + (\delta u \cdot \nabla)u + (u \cdot \nabla)\delta u - \dfrac{1}{Re}\Delta \delta u + \nabla \delta \pi = -\lambda(x)\delta u & \text{in } Q, \\ \nabla \cdot \delta u = 0 & \text{in } Q, \\ \delta u|_{t=0} = 0, \end{cases} \tag{51}$$

with the boundary conditions

$$\begin{aligned} \delta u|_{x=-x_l/2} &= \delta u|_{x=x_l/2}, \\ \delta u|_{z=-z_l/2} &= \delta u|_{z=z_l/2}, \\ \delta u|_{\Gamma_u} &= 0, \\ \delta u|_{\Gamma_c} &= n\delta v_c, \\ \delta u|_{\Gamma_l \setminus \Gamma_c} &= 0, \end{aligned} \tag{52}$$

where

$$\delta v_c(x,z,t) = \begin{cases} \delta\varphi_l^T \psi_l = \displaystyle\sum_{m=1}^{M} \delta\varphi_{l,m}(t)\psi_{l,m}(x,z) & \text{in } (T_1^c, T_2^c), \\ 0 & \text{otherwise.} \end{cases} \tag{53}$$

Now, let us consider the adjoint variable $p = p(x,y,z,t)$ and the adjoint pressure $\sigma = \sigma(x,y,z,t)$ and require p to satisfy the boundary conditions:

$$\begin{aligned} p|_{x=-x_l/2} &= p|_{x=x_l/2}, \\ p|_{z=-z_l/2} &= p|_{z=z_l/2}, \\ p|_{\Gamma_l} &= 0, \\ p|_{\Gamma_u} &= 0. \end{aligned} \tag{31}$$

As for the free-stream condition in the Navier–Stokes equations we actually use the Neumann condition

$$\left.\frac{\partial p}{\partial n}\right|_{\Gamma_u} = 0, \tag{32}$$

instead of the Dirichlet condition in the numerical simulations. See section 2.3 for more details regarding the boundary condition.

By multiplying the first equation in (51) with p and then integrating over Q we obtain

$$\int_Q p \cdot \Bigg(\underbrace{\frac{\partial \delta u}{\partial t}}_{1} + \underbrace{(\delta u \cdot \nabla)u}_{2} + \underbrace{(u \cdot \nabla)\delta u}_{3} \\ \underbrace{-\frac{1}{Re}\Delta \delta u + \nabla \delta \pi}_{4} + \underbrace{\lambda(x)\delta u}_{5} \Bigg) \mathrm{d}Q = 0. \tag{54}$$

We apply integration by parts in space and time to move the derivatives from u to the adjoint variable p. For clarity we perform this step by step for each term. The first term gives

$$\begin{aligned}\int_Q p \cdot \frac{\partial \delta u}{\partial t}\,\mathrm{d}Q &= \int_\Omega \left(p(T)\cdot\delta u(T) - p(0)\cdot\delta u(0)\right)\mathrm{d}\Omega \\ &\quad - \int_Q \frac{\partial p}{\partial t}\cdot\delta u\,\mathrm{d}Q \\ &= \int_\Omega p(T)\cdot\delta u(T)\,\mathrm{d}\Omega - \int_Q \frac{\partial p}{\partial t}\cdot\delta u\,\mathrm{d}Q,\end{aligned} \tag{55}$$

where we have used the fact that $\delta u(t=0)=0$. Next, we consider the fourth term

$$\begin{aligned}&-\frac{1}{Re}\int_Q p\cdot\Delta\delta u\,\mathrm{d}Q + \int_Q p\cdot\nabla\delta\pi\,\mathrm{d}Q \\ &\quad= -\frac{1}{Re}\int_0^T\left[\int_\Gamma p\cdot\frac{\partial\delta u}{\partial n}\,\mathrm{d}\Gamma + \int_\Omega \nabla p : \nabla\delta u\,\mathrm{d}\Omega\right]\mathrm{d}t \\ &\qquad+\int_0^T\left[\int_\Gamma p\cdot n\,\delta\pi\,\mathrm{d}\Gamma - \int_\Omega \nabla\cdot p\,\delta\pi\,\mathrm{d}\Omega\right]\mathrm{d}t \\ &\quad= \int_0^T\int_{\Gamma_u} p\cdot\left(n\,\delta\pi - \frac{1}{Re}\frac{\partial\delta u}{\partial n}\right)\mathrm{d}\Gamma\,\mathrm{d}t + \frac{1}{Re}\int_0^T\int_\Gamma \frac{\partial p}{\partial n}\cdot\delta u\,\mathrm{d}\Gamma\,\mathrm{d}t \\ &\qquad-\frac{1}{Re}\int_Q \Delta p\cdot\delta u\,\mathrm{d}Q - \int_Q \nabla\cdot p\,\delta\pi\,\mathrm{d}Q \\ &\quad= \frac{1}{Re}\int_0^T\int_{\Gamma_u}\frac{\partial p}{\partial n}\cdot\delta u\,\mathrm{d}\Gamma\,\mathrm{d}t + \frac{1}{Re}\int_{T_1^c}^{T_2^c}\left[\delta\varphi_l^T\int_{\Gamma_l}\psi_l\nabla p_2\cdot n\,\mathrm{d}\Gamma\right]\mathrm{d}t \\ &\qquad-\frac{1}{Re}\int_Q \Delta p\cdot\delta u\,\mathrm{d}Q - \int_Q \nabla\cdot p\,\delta\pi\,\mathrm{d}Q,\end{aligned} \tag{56}$$

where $p=(p_1,p_2,p_3)$. In the second equality we used the boundary condition (31) for p on Γ_l and enforced symmetry. In the third equality the condition for δu on Γ_l in (52) was used. We also assumed that p goes to zero on Γ_u. The : denotes a complete contraction defined as

$$\nabla p : \nabla\delta u = \sum_{i,j=1}^{3}\frac{\partial(e_i\cdot p)}{\partial x_j}\frac{\partial(e_i\cdot\,\delta u)}{\partial x_j}. \tag{12}$$

The next term to rewrite, in relation (54), is the second term

$$\int_Q p\cdot(\delta u\cdot\nabla)u\,\mathrm{d}Q = \int_Q (\nabla u)^T p\cdot\delta u\,\mathrm{d}Q. \tag{57}$$

Finally, we rewrite the third term in (54)

$$\begin{aligned}
&\int_Q p\cdot(u\cdot\nabla)\delta u\,\mathrm{d}Q \\
&\quad=\int_0^T\!\!\int_\Gamma (p\cdot\delta u)(n\cdot u)\,\mathrm{d}\Gamma\,\mathrm{d}t \\
&\qquad-\int_Q (p\cdot\delta u)(\nabla\cdot u)\,\mathrm{d}Q-\int_Q (u\cdot\nabla)p\cdot\delta u\,\mathrm{d}Q \\
&\quad=\int_0^T\!\!\int_{\Gamma_u} (p\cdot\delta u)(n\cdot u)\,\mathrm{d}\Gamma\,\mathrm{d}t-\int_Q (u\cdot\nabla)p\cdot\delta u\,\mathrm{d}Q,
\end{aligned} \tag{58}$$

where we have used the continuity condition on u and the boundary conditions (31) for p on Γ_l. The fifth term needs no rewriting.

Substituting (55), (56), (57) and (58) into (54) yields

$$\begin{aligned}
&\int_\Omega p(T)\cdot\delta u(T)\,\mathrm{d}\Omega+\frac{1}{Re}\int_{T_1^c}^{T_2^c}\left[\delta\varphi_l^T\int_{\Gamma_l}\psi_l\nabla p_2\cdot n\,\mathrm{d}\Gamma\right]\mathrm{d}t \\
&\quad+\int_Q \delta u\cdot\left(-\frac{\partial p}{\partial t}+(\nabla u)^T p-(u\cdot\nabla)p-\frac{1}{Re}\Delta p+\lambda(x)p\right)\mathrm{d}Q \\
&\quad-\int_Q \delta\pi\nabla\cdot p\,\mathrm{d}Q+\frac{1}{Re}\int_0^T\!\!\int_{\Gamma_u}\frac{\partial p}{\partial n}\cdot\delta u\,\mathrm{d}\Gamma\,\mathrm{d}t \\
&\quad+\int_0^T\!\!\int_{\Gamma_u}(n\cdot u)(p\cdot\delta u)\,\mathrm{d}\Gamma\,\mathrm{d}t=0.
\end{aligned} \tag{59}$$

Now, require p to satisfy the adjoint equations:

$$\begin{cases}
-\dfrac{\partial p}{\partial t}+(\nabla u)^T p-(u\cdot\nabla)p & \\
\quad-\dfrac{1}{Re}\Delta p+\lambda(x)p+\nabla\sigma=\begin{cases} u-u_T & \text{in } (T_1^o,T_2^o)\times\Omega_o \\ 0 & \text{otherwise}\end{cases} & \text{in } Q, \\
\nabla\cdot p=0 & \text{in } Q, \\
p|_{t=T}=0, &
\end{cases} \tag{30}$$

with the boundary conditions (31). With these assumptions equation (59) becomes

$$\begin{aligned}
&\int_{T_1^o}^{T_2^o}\!\!\int_{\Omega_o}\delta u\cdot(u-u_T)\,\mathrm{d}Q-\int_Q\delta u\cdot\nabla\sigma\,\mathrm{d}Q \\
&\qquad+\frac{1}{Re}\int_0^T\!\!\int_{\Gamma_u}\frac{\partial p}{\partial n}\cdot\delta u\,\mathrm{d}\Gamma\,\mathrm{d}t+\int_0^T\!\!\int_{\Gamma_u}(n\cdot u)(p\cdot\delta u)\,\mathrm{d}\Gamma\,\mathrm{d}t=0,
\end{aligned} \tag{60}$$

since p and $\partial p_2/\partial n$ is zero on the boundary $y = 0$ due to the no-slip and continuity conditions. The second term in (60) can be rewritten

$$\begin{aligned} -\int_Q \delta u \cdot \nabla\sigma \,\mathrm{d}Q &= -\int_0^T\!\!\int_\Gamma \delta u \cdot n\,\sigma \,\mathrm{d}\Gamma\,\mathrm{d}t + \int_Q \nabla\cdot\delta u\,\sigma\,\mathrm{d}Q \\ &= -\int_0^T\!\!\int_\Gamma \delta u \cdot n\,\sigma\,\mathrm{d}\Gamma\,\mathrm{d}t, \end{aligned} \tag{61}$$

since $\nabla \cdot \delta u = 0$. The final step is now to substitute the terms involving δu. When that is done the second term in the perturbed objective function (50) can be replaced with terms involving $\delta\varphi$. Since δu is known on parts of the boundary we can proceed as follows

$$\begin{aligned} &-\int_0^T\!\!\int_\Gamma \delta u \cdot n\,\sigma\,\mathrm{d}\Gamma\,\mathrm{d}t \\ &\qquad = -\int_0^T\!\!\int_{\Gamma_u} \delta u \cdot n\,\sigma\,\mathrm{d}\Gamma\,\mathrm{d}t + \int_{T_1^c}^{T_2^c}\left[\delta\varphi_l^T \int_{\Gamma_c}\psi_l\sigma\,\mathrm{d}\Gamma\right]\mathrm{d}t. \end{aligned} \tag{62}$$

Combining equation (61) and (62) and inserting that into (60) yield

$$\begin{aligned} &\int_{T_1^o}^{T_2^o}\!\!\int_{\Omega_o} \delta u\cdot(u-u_T)\,\mathrm{d}Q + \int_0^T\!\!\int_{\Gamma_u} \delta u\cdot\left(\frac{1}{Re}\frac{\partial p}{\partial n} - \sigma n + (n\cdot u)p\right)\mathrm{d}\Gamma\,\mathrm{d}t \\ &\qquad + \int_{T_1^c}^{T_2^c}\left[\delta\varphi_l^T\int_{\Gamma_c}\psi_l\sigma\,\mathrm{d}\Gamma\right]\mathrm{d}t = 0. \end{aligned} \tag{63}$$

Applying the fourth boundary condition (31) for p together with the assumption that $p = 0$ and also $\sigma = 0$ on Γ_u we get

$$\int_{T_1^o}^{T_2^o}\!\!\int_{\Omega_o} \delta u\cdot(u-u_T)\,\mathrm{d}Q = -\int_{T_1^c}^{T_2^c}\left[\delta\varphi_l^T\int_{\Gamma_c}\psi_l\sigma\,\mathrm{d}\Gamma\right]\mathrm{d}t. \tag{64}$$

Remains only to substitute (64) into (50) which yields

$$\delta J(\varphi_l) = \left\langle \frac{\partial J}{\partial\varphi_l}, \delta\varphi_l\right\rangle = \int_{T_1^c}^{T_2^c}\delta\varphi_l^T\int_{\Gamma_c}\psi_l\left(\varepsilon\varphi_l^T\psi_l - \sigma\right)\mathrm{d}\Gamma\,\mathrm{d}t \tag{65}$$

where the gradient of the objective function can be identified as:

$$\frac{\partial J}{\partial\varphi_l} = \int_{\Gamma_c}\psi_l\left(\varepsilon\varphi_l^T\psi_l - \sigma\right)\mathrm{d}\Gamma. \tag{33}$$

This is exactly the same expression for the gradient as for the channel flow case, equation (22) and (23), except that this gradient is restricted to information from Γ_c.

References

[1] BERGGREN, M. 1998 Numerical solution of a flow-control problem: vorticity reduction by dynamic boundary action *SIAM J. Sci. Comput.*, **19** (3), 829–860.

[2] BEWLEY, T. R., MOIN, P., TEMAM, R. 2001. DNS-based predictive control of turbulence: an optimal target for feedback algorithms. *J. Fluid Mech.* **477**, 179–225.

[3] BYRD, R. H., PEIHUANG, L., NOCEDAL, J. & ZHU, C. 1994. A limited memory algorithm for bound constrained optimization *Technical Report NAM-08* Northwestern University.
`http://www.netlib.org/toms/778`

[4] CANUTO, C. HUSSAINI, M. Y., QUARTERONI, A. & ZANG, T. A. 1988. *Spectral methods in Fluid Dynamics* Springer Verlag.

[5] COLLIS, S. S., CHANG, Y., KELLOGG, S. & PRABHU, R. D. 2000 Large eddy simulation and turbulence control AIAA-paper 2000–2564.

[6] GLOWINSKI, R. & HE, J. 1998 On shape optimization and related issues *Computational Methods for Optimal Design and Control*, J. BORGGAARD *et al.* (eds), Birkhäuser, Boston, 151–179.

[7] GUNZBURGER, M. D. 1998 Sensitivities in computational methods for optimal flow control *Computational Methods for Optimal Design and Control*, J. BORGGAARD *et al.* (eds), Birkhä user, Boston, 197–236

[8] GUNZBURGER, M. D. 1995 *Flow control.* (M. D. GUNZBURGER editor) Springer Verlag, Berlin.

[9] HINZE, M. & KUNISCH, K. 2000 Three control methods for time dependent fluid flow. *Flow, Turbulence and Combustion* **65** (3/4), 273–298.

[10] HÖGBERG, M. & BERGGREN, M. 2000. Numerical investigation of different discretization approaches for optimal Control. *Flow, Turbulence and Combustion* **65** (3/4), 299–320.

[11] HÖGBERG, M. & BEWLEY, T. R. 2001. Spatially localized convolution kernels for decentralized control and estimation of plane channel flow. Submitted to *Automatica*.

[12] HÖGBERG, M. & Henningson, D. S. 2001. Linear optimal control applied to instabilities in spatial boundary layers. Submitted to *J. Fluid Mech.*

[13] HÖGBERG, M., HENNINGSON, D. S. & BERGGREN, M. 2000. Optimal control of bypass transition. In *Advances in turbulence VIII*, DOPAZO, C. *et al.* , editors.

[14] JOSLIN, R. D. , GUNZBURGER, M. D. & NICOLAIDES, R. A. 1997. Self-Contained Automated Methodology for Optimal Flow Control. *AIAA Journal*, **35** (5), 816–824.

[15] KIM, J. & LIM, J. 2000 A linear process in wall-bounded turbulent shear flows *Phys. Fluids* **12** (8), 1885–1888.

[16] LUNDBLADH, A., HENNINGSON, D. S. & JOHANSSON, A. V. 1992. An Efficient Spectral Integration Method for the Solution of the Navier–Stokes Equations *FFA TN* 1992-28.

[17] LUNDBLADH, A., BERLIN, S., SKOTE, M., HILDINGS, C., CHOI, J., KIM, J. & HENNINGSON, D. S. 1999 An efficient spectral method for simulation of incompressible flow over a flat plate. Technical report, Department of Mechanics, KTH, *TRITA-MEK* 1999:11.

[18] MORKOVIN, M. V. 1969. The many faces of transition. In *Viscous Drag Reduction* (WELLS, C. S., editor) Plenum Press.

[19] NORDSTRÖM, J., NORDIN, N. & HENNINGSON, D. S. 1999 The fringe region technique and the Fourier method used in the direct numerical simulation of spatially evolving viscous flows. *SIAM J. Sci. Comp.* **20** (4), 1365–1393.

[20] REDDY, S. C., SCHMID, P. J., BAGGETT, J. S. & HENNINGSON, D. S. 1998. On stability of streamwise streaks and transition thresholds in plane channel flows. *J. Fluid Mech.*, **365**, 269–303.

[21] SCHMID, P. J. & HENNINGSON, D. S. 2001. *Stability and transition in shear flows* Springer Verlag.

[22] SRITHARAN, S. S. 1998 *Optimal control of viscous flows.* (S. S. SRITHARAN editor) SIAM.

Issuing organisation
FOI – Swedish Defence Research Agency
Division of Aeronautics, FFA
SE-172 90 STOCKHOLM

Report number, ISRN
FOI-R–0182–SE

Report type
Scientific report

Month year
October 2001

Project number
A80 0140

Customers code
3. Aeronautical Research

Research area code
7. Vehicles

Sub area code
79. Interdisciplinary Project

Author(s)
Markus Högberg, Mattias Chevalier, Martin Berggren & Dan S. Henningson

Project manager
Dan Henningson

Approved by
Torsten Berglind
Head, Computational Aerodynamics Department

Scientifically and technically responsible
Dan Henningson
Professor

Report title
Optimal control in wall bounded flows

Abstract

Optimal control of transition in channel flow and boundary layer flow is attempted. First the optimization problem is stated and the corresponding adjoint equations used to compute the gradient of the objective function are derived for both the channel flow and boundary layer flow problems. Implementation and numerical issues are discussed. The governing equations are the incompressible Navier–Stokes equations with appropriate boundary conditions for the two cases. The boundary condition on the wall normal velocity at the walls of the channel, or at the single wall in the boundary layer case, is used as control and is determined in the iterative optimization procedure. The objective function used for the optimization problem contains the perturbation energy and a regularization term containing the control. The optimization problem is formulated using the primitive variables — velocity and pressure — and is then rewritten in a formulation containing only the wall normal velocity and the wall normal vorticity. An existing solver for the incompressible Navier–Stokes equations using this formulation can then also be used to solve the associated adjoint problem. The implementation is straightforward using this formulation and the efficiency of the original solver is maintained. To test the performance of the solver of the optimization problem, it is applied on different stages of the oblique transition scenario in the channel flow case. In a parallel Falkner–Skan–Cooke flow successful control of an inviscid instability is reported, and in the spatial Blasius flow the energy growth of a Tollmien–Schlichting wave is efficiently inhibited.

Keywords
shear flow, optimal control, adjoint equations

Further bibliographic information

ISSN
ISSN 1650-1942

Pages
39

Language
English

Price
Acc. to price list

Security classification
Open

Utgivare	Rapportnummer, ISRN	Klassificering
Totalförsvarets Forskningsinstitut – FOI Avdelningen för Flygteknik, FFA SE-172 90 STOCKHOLM	FOI-R–0182–SE	Vetenskaplig rapport
	Månad år Oktober 2001	Projektnummer A80 0140
	Verksamhetsgren 3. Flygteknisk forskning	
	Forskningsområde 7. Bemannade och obemannade farkoster	
	Delområde 79. Breda projekt bemannade och obemannade farkoster	

Författare	Projektledare
Markus Högberg, Mattias Chevalier, Martin Berggren & Dan S. Henningson	Dan Henningson
	Godkänd av Torsten Berglind Chef, Institutionen för beräkningsaerodynamik
	Tekniskt och/eller vetenskapligt ansvarig Dan Henningson Professor

Rapporttitel

Optimal styrning i väggbunden skjuvströmning

Sammanfattning

Försök av optimal styrning av omslag till turbulens i kanal och gränsskiktsströmning har gjorts. Först formuleras optimeringsproblemet och sedan härleds motsvarande adjunkta ekvationer för att beräkna gradienten av objektsfunktionen för både kanal och gränsskiktsproblemet. Implementation och numeriska problem diskuteras. De ekvationer som löses är Navier–Stokes ekvationer för inkompressibel strömning med adekvata randvillkor för de två fallen. Randvillkoret på normalhastigheten på kanalens väggar eller på den enda väggen i gränsskiktsfallet används som kontroll och bestäms genom en iterativ optimeringsprocedur. Objektsfunktionen som används för optimeringsproblemet innehåller störningsenergin och en regulariseringsterm på kontrollen. Optimeringsproblemet formuleras i primitiva variabler — hastighet och tryck — och skrivs sedan om så att endast normalhastighet och normalvorticitet ingår. En existerande lösare för inkompressibla Navier–Stokes ekvationer för denna formulering av ekvationerna kan sedan också användas för de associerade adjunkta ekvationerna. Implementationen har gjorts så att effektiviteten av den ursprungliga lösaren bibehålls. För att undersöka prestandan av lösaren för optimeringsproblemet prövades kontroll av olika faser i omslagsprocessen för två sneda vågor i kanalströmning. I ett parallellt Falkner-Skan–Cooke flöde rapporteras kontroll av en inviskös instabilitet och i ett spatiellt Blasius gränsskikt dämpas effektivt energitillväxten av en Tollmien-Schlichting våg.

Nyckelord

skjuvströmning, optimal styrning, adjunkta ekvationer

Övriga bibliografiska uppgifter

ISSN	Antal sidor	Språk
ISSN 1650-1942	39	Engelska
Distribution enligt missiv Distribution	Pris Enligt prislista	
	Sekretess Öppen	